Journal of Cleaner Production 288 (2021) 125687

Contents lists available at ScienceDirect

Journal of Cleaner Production

journal homepage: www.elsevier.com/locate/jclepro

Soil mercury pollution caused by typical anthropogenic sources in China: Evidence from stable mercury isotope measurement and receptor model analysis

Zhengcheng Song [a, 1], Chuan Wang [a, b, 1], Li Ding [c], Min Chen [c], Yanxin Hu [d], Ping Li [a, e, *], Leiming Zhang [f], Xinbin Feng [a, e]

[a] State Key Laboratory of Environmental Geochemistry, Institute of Geochemistry, Chinese Academy of Sciences, Guiyang, 550081, China
[b] University of Chinese Academy of Sciences, Beijing, 100049, China
[c] School of Public Health, Guizhou Medical University, Guiyang, 550025, China
[d] School of Chemistry and Chemical Engineering, Guizhou University, Guiyang, 550025, China
[e] CAS Center for Excellence in Quaternary Science and Global Change, Xi'an, 710061, China
[f] Air Quality Research Division, Science and Technology Branch, Environment and Climate Change Canada, Toronto, M3H 5T4, Canada

ARTICLE INFO

Article history:
Received 19 August 2020
Received in revised form
17 November 2020
Accepted 23 December 2020

Handling editor: Zhifu Mi

Keywords:
Anthropogenic mercury emission
Soil mercury
Mercury isotope
Source apportionment

ABSTRACT

Human activities have caused serious soil mercury (Hg) pollution in industrial areas worldwide. Abatement of soil Hg pollution requires knowledge of Hg sources and transport pathways across various environmental media. In this study, four areas containing typical anthropogenic Hg emissions in China were selected to evaluate soil Hg pollution. Results showed that soil Hg contents were significantly elevated in areas of Hg mining, gold mining, and zinc smelting, but only slightly elevated in an area of coal-fired power plant, with averages of 44.0, 1.17, 0.73, and 0.14 μg g^{-1} (dry weight) in these four areas, respectively. The average percentage contributions from these anthropogenic sources to soil Hg in surrounding areas were estimated to be 92.2 ± 9.70% from Hg mining (among which 77.6 ± 12.0% from unroasted Hg ore and 14.6 ± 7.50% from Hg calcine), 63.5 ± 0.83% from the zinc smelting, 41.6 ± 1.90% from gold mining, and 21.1 ± 3.58% from coal-fired power plant. Atmospheric deposition was speculated to be the main pathway for soil Hg contamination, but mercury mining area contained significant runoff accumulation. Speciation and concentration of Hg in emission gas are crucial factors for Hg pollution in surrounding soils, because of short residence time of Hg^{2+}/Hg_p in the atmosphere. The results obtained in this study can provide scientific advices for risk assessment and soil remediation of Hg in China and other regions with similar industries.

1. Introduction

Mercury (Hg) is one of the top ten toxic chemicals concerning human health (WHO, 2018). Mercury is released from both natural and anthropogenic sources, and can undergo long range transport in the atmosphere in the form of Hg^0 (Selin, 2009). Mercury input to aquatic and terrestrial ecosystems can be methylated into methylmercury (MeHg) (Parks et al., 2013), which can then be bioaccumulated in food products that are commonly consumed by general population, imposing potential human health concerns (Driscoll et al., 2013; Wright et al., 2018). For example, MeHg exposure can cause neurocognitive deficits in fetuses and cardiovascular effects in adults (Roman et al., 2011; Hu et al., 2018; Liu et al., 2019; Chen et al., 2019). To mitigate impacts of Hg exposure to human health, the *Minamata Convention on Mercury* was entered into force in August 2017.

Soil is the largest Hg reservoir globally (Wang et al., 2019), and is also a major natural source for atmospheric Hg (UNEP, 2019). Agricultural products cultivated on Hg contaminated soils may contain high-levels of MeHg (Li et al., 2009, 2011, 2017a). Although seafood consumption is recognized as the main pathway of human MeHg exposure worldwide, consumption of MeHg contaminated rice contribute major human MeHg exposure in Hg contaminated

* Corresponding author. State Key Laboratory of Environmental Geochemistry, Institute of Geochemistry, Chinese Academy of Sciences, Guiyang, 550081, China.
E-mail address: liping@mail.gyig.ac.cn (P. Li).
[1] These authors contribute equally.

https://doi.org/10.1016/j.jclepro.2020.125687
0959-6526/

areas where local residents seldom consume fish, causing high health risks to local population (Zhang et al., 2010; Li et al., 2015). Agricultural planning is, to some extent, an effective strategy for minimizing MeHg exposure risks in Hg contaminated areas (Xia et al., 2020). However, to avoid persistent soil Hg pollution and subsequent human MeHg exposure, sources of soil Hg need to be first identified and Hg emissions from these sources can then be controlled by optimizing the major emission processes. Common sources of Hg in soil include atmospheric deposition, anthropogenic input, and natural geological origin (Luo et al., 2009; Zhou et al., 2018). The relative contributions of these sources to soil Hg contents have not been quantitatively assessed, especially in Hg mining and other industrial areas where anthropogenic Hg sources are dominant.

Mercury stable isotope is an effective tool for tracing the pollution sources and environmental processes (Kwon et al., 2020). Mercury isotope undergoes both mass dependent fractionation (MDF, reported as δ^{202}Hg) and mass independent fractionation (MIF, reported as Δ^{199}Hg, Δ^{201}Hg, and Δ^{200}Hg) in the environment. MDF can occur in many physical, chemical, and biological processes (Kwon et al., 2020) while MIF occurs only in several specific processes, such as photochemical reduction of Hg^{2+} (Zheng and Hintelmann, 2010) and photodegradation of MeHg (Bergquist and Blum, 2007). Mixing models based on MDF and MIF data have been developed for quantitative source apportionment of Hg in soil (Estrade et al., 2011), sediment (Yin et al., 2015), and atmosphere (Fu et al., 2016). Receptor model is another effective technique for source apportionment, which can obtain quantitative contribution rates through the intrinsic mathematical processes without source profiles (Cheng et al., 2013, 2015). Receptor model approach has been applied on the source appointment of pollutants in soil and sediments, such as heavy metal (Huang et al., 2018; Brady et al., 2014) and polychlorinated biphenyls (Pornsawai et al., 2013).

China has most anthropogenic Hg emissions worldwide, e.g., releasing 538 t Hg into the atmosphere in 2010 (Zhang et al., 2015). Coal combustion, non-ferrous metal smelting, and cement production have been identified as the primary Hg emission sectors, with the emission of 253.8t, 97.4t, 98.3t of Hg in 2010, respectively (Zhang et al., 2015). However, to what extent the major anthropogenic Hg sources impact soil Hg is unknown. To fill this knowledge gap, this study collected soil Hg samples in four selected areas that contain typical anthropogenic Hg sources (zinc smelting, gold mining, coal-fired power plant, and Hg mining areas) in China. The analyzed Hg isotopic data were applied with two receptor models for apportioning sources of and relative contributions to soil Hg. The results obtained in this study can provide scientific advices for risk assessment and soil remediation of Hg in China and other regions with similar industries.

2. Materials and methods

2.1. Description of sampling areas and measurements

Four areas were selected in this study for soil sampling, with each area containing one type of typical source of atmospheric Hg emissions. The first one is zinc smelter area (ZSA) with the smelter (27°52′23.06″ N, 113°05′08.40″ E, operation started in 1950s) mainly producing zinc, lead, and alloy products, which produces one of the largest amounts of non-ferrous metals in China. The second one is coal-fired power plant area (CFPPA) with the plant (26°12′53.01″N, 105°41′31.65″ E, operation started in 1970s) having the largest single unit capacity in southwest China. The third one is gold mining area (GMA) with the mining (25°32′09.82″ N, 105°32′48.95″ E, operation started in 1990s) being one of the largest Carlin-type gold deposits in China. And the fourth one is mercury mining area (MMA) with a large-scale and long-history Hg mining (27°32.940′ N, 109°12.838′ E, operation period during 221 BC - 2002). Detailed descriptions of these sampling areas are provided in Section 1 of the Support Information (SI). From October to December 2017, 33, 31, and 29 surface soil samples were collected from croplands within 5 km of ZSA, CFPPA, and GMA, respectively, and 3 soil profiles were also collected from each of the above three areas. During the same period, 14 surface soil samples and 4 soil profiles were collected in the paddy field of MMA. Dust samples on streets, windowsills, and guardrails and agricultural fertilizers from farmland and local stores were collected in every area. Coal samples were collected from the coal-fired power plant, and crude zinc ore and fly ash samples were collected from the zinc smelter.

Total gaseous mercury (TGM) concentrations were measured at all the sampling sites by a Lumex RA-915+ portable analyzer at 1 s time resolution and with a detection limit of 1–2 ng m^{-3}, and reported as 5-min mean values. The measurement in each area was conducted at different time. Prior to measurement, this instrument was manually calibrated using its internal test cell and the inlet was kept at ~20 cm from the ground. Total Hg (THg) contents in solid samples were analyzed by the RA-915 analyzer, equipped with a pyrolysis attachment (PYRO-915+), with a detection limit of 1 ng g^{-1} (Zhou et al., 2013). For solid samples with relatively low THg concentrations, THg contents were determined by acid digestion and cold vapor atomic fluorescence spectrometry (CVAFS, Tekran 2500).

Hg isotopes were analyzed by a Neptune Plus multi collector inductively coupled plasma mass spectrometer at the State Key Laboratory of Environmental Geochemistry, Institute of Geochemistry, Chinese Academy of Sciences, as described in Yin et al. (2016). Internal Hg isotope correction was employed for Hg isotopic measurement using standard Tl solution (NIST SRM 997). Approximately 0.2 g sample powder was digested (95 °C, 3 h) in 5 mL aqua regia ($HCl:HNO_3 = 3:1$, v:v), and kept for at least 24 h, then BrCl was added to the solution for fully oxidation. Digests were diluted to 0.5 ng mL^{-1} Hg in 10–20% (v/v) aqua regia. δ^{202}Hg, Δ^{199}Hg, and Δ^{201}Hg were calculated relative to NIST SRM 3133 (Blum and Bergquist, 2007).

Trace elements were determined by acid digestion and an inductively-coupled plasma mass spectrometer (Thermo Fisher, ICP-MS X2), which utilized 4 internal standards: ^{103}Rh, ^{115}In, ^{187}Re, ^{209}Bi.

2.2. Quality control of measurements

Quality controls of measurements consisted of method blanks, certified reference materials (CRMs), and blind duplicates. THg analytical accuracy was evaluated by measuring GBW07405 (soil, n = 6), CRM021 (soil, n = 6), and CRM024 (soil, n = 6). Averages of THg concentrations obtained in CRMs (GBW07405, CRM021, and CRM024) were 0.28 ± 0.01 μg g^{-1}, 4.69 ± 0.221 μg g^{-1}, and 0.710 ± 0.06 μg g^{-1}, respectively, which were consistent with the certified values of 0.29 ± 0.03 μg g^{-1}, 4.70 ± 0.179 μg g^{-1}, and 0.710 μg g^{-1}, respectively. The average relative difference was <10% for THg in duplicate samples.

Certified reference materials NIST SRM 2711 (n = 3) were similarly prepared for Hg isotope analysis. Analytical uncertainties were estimated based on replication of NIST SRM 3133 solutions. Our results of NIST SRM 2711 (δ^{202}Hg: −0.28 ± 0.02‰, Δ^{199}Hg: −0.27 ± 0.03‰, and Δ^{201}Hg: −0.23 ± 0.01‰) are consistent with previous studies (Blum and Bergquist, 2007; Yin et al., 2016).

2.3. Mercury isotope calculation

MDF results were calculated as following:

$$\delta^{xxx}Hg_{sample}\ (‰) = [(^{xxx/198}Hg_{sample}/^{xxx/198}Hg_{NIST3133}) - 1] \times 1000 \quad (1)$$

where xxx is 199, 200, 201, or 202.

MIF was defined using capital delta (Δ) notation and calculated as:

$$\Delta^{199}Hg = \delta^{199}Hg - \delta^{202}Hg \times 0.252 \quad (2)$$

$$\Delta^{200}Hg = \delta^{200}Hg - \delta^{202}Hg \times 0.502 \quad (3)$$

$$\Delta^{201}Hg = \delta^{201}Hg - \delta^{202}Hg \times 0.752 \quad (4)$$

2.4. Source apportionment analysis

Source apportionment analyses were conducted using Hg isotope and receptor model approaches. The Hg isotope approach needs accurate isotope values of each source, while the receptor model requires detailed information of the contaminated soil. Reliable results of source apportionment can be verified by these two methods.

2.4.1. Hg isotope approach

A binary mixing model was established to evaluate the relative contribution of two sources using Eqs. (5) and (6) (Estrade et al., 2011; Yin et al., 2013):

$$^{xxx}Hg_{soil} = F_{ant} \times {}^{xxx}Hg_{ant} + F_{nat} \times {}^{xxx}Hg_{nat} \quad (5)$$

$$1 = F_{ant} + F_{nat} \quad (6)$$

Where *ant* and *nat* refer to anthropogenic and natural background origins, respectively. F_{ant} and F_{nat} represent the fraction of Hg deriving from anthropogenic sources or end members (including zinc smelting (F_{zs}), coal-fired (F_{coal}), and gold mining (F_{gold})).

A triple mixing model was established (Eq.s (7)–(9)) to calculate the relative fractions of the three sources in soil Hg of MMA:

$$\delta^{202}Hg_{soil} = F_{ore} \times \delta^{202}Hg_{ore} + F_{cal} \times \delta^{202}Hg_{cal} + F_{nat} \times \delta^{202}Hg_{nat} \quad (7)$$

$$THg_{soil} = F_{ore} \times THg_{ore} + F_{cal} \times THg_{cal} + F_{nat} \times THg_{nat} \quad (8)$$

$$1 = F_{ore} + F_{cal} + F_{nat} \quad (9)$$

where subscripts *ore, cal,* and *nat* refer to origins of unroasted Hg ore, Hg calcine, and natural source, respectively.

2.4.2. Receptor model approach

The positive matrix factorization (PMF) is an apportionment modeling tool recommended by the U.S Environmental Protection Agency (USEPA). Non-negativity constraints and use of uncertainty to weigh each data point individually are the registered remarkable features (Norris et al., 2014). A correlation matrix and covariance matrix were used to simplify the initial high dimensional variables. In this study, PMF 5.0 was adopted according to the corresponding user guide (USEPA, 2014). The uncertainties were assigned to be 15% following the study of Pornsawai et al. (2013).

The principal component analysis/absolute principal component scores (PCA/APCS) receptor model is composed of the PCA and APCS techniques. The PCA has the ability to reduce the large dataset into several principal components (PCs) that explain most of the variance (Brady et al., 2014). Each of the PCs shows a characteristic group of elements that can be linked to a source. APCS are used to determine the quantitative links of the sources identified from the PCA contributed to pollutants. Details about the APCS were described by Thurston and Spengler (1985).

The receptor models described above have different intrinsic mathematical processes, which gain the PCs in PCA/APCS and factors (Fs) in PMF. The PCs and Fs are characterized by different elements, which can be used to infer the sources. In this study, we mainly discuss the relative contributions from emission sectors and geogenic background (details in SI and Sections 2 and 3).

3. Results and discussion

3.1. THg concentrations

THg concentrations in surface soil samples of ZSA averaged at 0.73 ± 0.65 μg g^{-1} (0.04–2.88 μg g^{-1}, dry weight, n = 33) (Table 1), which are comparable with the results of previous studies also conducted in the same area, with the mean of 1.09 μg g^{-1} (0.38–2.89 μg g^{-1}) by Li et al. (2011) and the mean of 1.54 μg g^{-1} (0.62–2.61 μg g^{-1}) by Wu et al. (2014). These values indicated moderate Hg contamination in soils of ZSA when compared with the regional background value of 0.116 μg g^{-1} (CNEMC, 1990). 61.5% (8/13) of paddy soils (standard: >0.6 μg g^{-1}, with pH ≤ 7.5) and 10.0% (2/20) of dry-land soils (standard: >2.4 μg g^{-1}, with pH ≤ 7.5) exceeded the China's soil risk screening values (MEE, 2018). Crude ore, dust, and fly ash samples also showed high Hg levels, with mean concentrations of 65.3 ± 16.2 μg g^{-1} (n = 4), 2.84 ± 3.85 μg g^{-1} (n = 9), and 2.60 ± 4.04 μg g^{-1} (n = 4), respectively (Table A.1).

THg concentrations in surface soils of CFPPA averaged at 0.14 ± 0.05 μg g^{-1} (0.07–0.25 μg g^{-1}, n = 31), which showed slight elevation comparing with background value (0.110 μg g^{-1}, CNEMC 1990), and are lower than those reported for other similar areas in China, e.g., 0.606 μg g^{-1} (average) in Baoji (Yang and Wang, 2008) and 0.344 μg g^{-1} (average) in Heilongjiang (Li et al., 2017b). THg concentrations in coal samples and dust samples of CFPPA averaged at 0.15 ± 0.02 μg g^{-1} (n = 4) and 0.037 ± 0.035 μg g^{-1} (n = 11), respectively.

THg concentrations in surface soil samples and dust samples in GMA averaged at 1.17 ± 2.19 μg g^{-1} (0.11–7.77 μg g^{-1}, n = 29) and 2.21 ± 3.62 μg g^{-1} (0.202–11.6 μg g^{-1}, n = 9), respectively, which revealed moderate soil Hg contamination in this area comparing with background value (0.110 μg g^{-1}, CNEMC 1990). 17.2% (5/29) of surface soil samples would be classified as Hg contamination according to China's soil risk screening values (>2.4 μg g^{-1}, with pH ≤ 7.5, for dry-land soil) (MEE, 2018).

THg concentrations in surface soils of MMA averaged at 44.0 ± 23.2 μg g^{-1} (10.9–113 μg g^{-1}, n = 14), and all exceeded the China's soil risk intervention values for Hg (4.0 μg g^{-1}, with 6.5 < pH ≤ 7.5) (MEE, 2018), which indicated heavy soil Hg pollution in this area. THg concentrations in 2 dust samples were 17.4 and 25.1 μg g^{-1}, respectively, which were the highest values among all the dust samples collected in the four areas. High THg contents were found in the unroasted ore with an average of 1150 μg g^{-1} in the same area (Yin et al., 2013), which were 100–1000 times higher than those in soil samples. The mean THg content in roasted ores

Table 1
THg concentrations in soil samples in the four study areas (μg g^{-1}, dry weight).

Area	n	Geomean	Mean	STD	Min	Max
ZSA	33	0.54	0.73	0.65	0.04	2.88
CFPPA	31	0.13	0.14	0.05	0.07	0.25
GMA	29	0.42	1.17	2.19	0.11	7.77
MMA	14	34.2	44.0	23.2	10.9	113

was 56.9 μg g^{-1}, indicating high amounts of Hg remained in the mine waste calcine, even after the high temperature smelting process (Yin et al., 2013).

Based on the data discussed above, heavy soil Hg pollution in MMA, moderate soil Hg pollution in GMA and ZSA, and light soil Hg pollution in CFPPA were detected. Although Hg mining activities in MMA have been ceased since 2002, historical long-time large-scale Hg mining have already caused serious soil Hg pollution in the surrounding areas. In addition, large quantities of Hg mine waste (calcine) can continuously release Hg to the surrounding environment through atmosphere deposition and water flow (Li et al., 2008). The above factors explained the heaviest soil Hg pollution in MMA among the four areas. The moderate soil Hg pollution in GMA and ZSA were likely caused by the relatively high Hg contents in flue gas released from these facilities, especially considering the emitted Hg is mainly in the form of Hg(II) (Zhang et al., 2012; Wang et al., 2010; Wu et al., 2018) that can quickly deposit in the vicinity of the facilities (Biester et al., 2002). For example, Hg contents in flue gas from two zinc smelters in China were previously reported to be 34.5 and 74.8 μg m^{-3}, respectively (Zhang et al., 2012), while those in flue gas from gold roasting processes were reported to average at 6 and 50 μg m^{-3} in two gold smelters (Wu et al., 2018). In comparison, relatively low Hg contents in flue gas of CFPPs in China were reported, e.g., from 0.052 to 9.16 μg m^{-3} due to the installed purification facilities, such as selective catalytic reduction (SCR), wet electrostatic precipitators (WESPs), and/or advanced electrostatic fabric filters (ESP-FFs) (Zhao et al., 2019). Besides, the emitted Hg from CFPPs is mainly in the form of Hg^0, which has relatively low impact on local environment. Thus, the lightest Hg soil pollution was found in CFPPA among the four areas. It should be noted that Hg in CFPPs is mostly removed before being emitted into the atmosphere as a co-benefit of air pollution control policy.

3.2. Spatial and vertical distribution

Spatial distributions of THg concentration in surface soils exhibited highest concentrations within a distance of about 1.5–2.0 km from the emission sources in the southwest and northwest of ZSA, west of CFPPA, and southeast of GMA (Fig. 1). The regions with high THg concentration were not distributed in the trade-wind zone in ZSA and GMA, and these patterns also related to the local topography, as the topography were also important factors affecting the pollutant's transportation. The spatial distributions of soil Hg reflected typical patterns of atmospheric Hg deposition surrounding point sources, similar to what were reported previously in chlor-alkali plant (Song et al., 2018) and Zn/Pb smelter in China (Wu et al., 2014). The above spatial distribution pattern was not observed in surface soil THg in MMA because of the relatively small research area investigated.

THg concentrations in soil profiles (SP) generally exhibited significantly elevated Hg levels near the surface (0–20 cm) in ZSA and CFPPA, suggesting that Hg in surface soils were mainly originated from atmospheric deposition (SP1-SP6, Fig. 2). However, in GMA and MMA, THg concentrations firstly increased with soil depth and reached the maximum at 20–40 cm in SP7, SP8, SP12, and SP13, which was likely caused by reclamation after mining activities and human disturbances.

TGM concentrations in ZSA, CFPPA, and GMA averaged at 10.8 ± 5.32 ng m^{-3} (3.8–22.6 ng m^{-3}, n = 33), 5.17 ± 1.8 ng m^{-3} (2.17–9.25 ng m^{-3}, n = 26), and 4.55 ± 1.51 ng m^{-3} (1.71–7.07 ng m^{-3}, n = 29), respectively, which are below the national standard for ambient air quality in China (50 ng m^{-3}) (MEP, 2012) and comparable with those in urban areas of China (5.4–18.4 ng m^{-3}, Fang et al., 2001; Wang et al., 2007). TGM concentrations in MMA ranged from 17 to 80 ng m^{-3}, while the maximum value exceeded national standard of 50 ng m^{-3}. TGM concentrations gradually decreased from the west (close to the mine waste heap) to the east in MMA (Fig. A.2g). TGM concentrations in the mine waste heap were detected as high as 254–276 ng m^{-3}, suggesting the mine waste heap was a significant emission source of atmospheric Hg. Since the spatial distributions of TGM concentrations were significantly influenced by instantaneous meteorological conditions, the short-term TGM distribution of this study may not agree well with the spatial distributions of soil Hg. And long-term observations are needed to improve this in future study.

Overall, the spatial distribution of soil Hg in ZSA, GMA, and CFPPA reflected typical impacts from the point sources, where the Hg was released from the chimneys, transported to the surrounding areas under the influence of local meteorological and topographical conditions, and finally deposited to the surface soils.

3.3. Hg isotopic composition

δ^{202}Hg values in sphalerite (Zn ore), fly ash, soil, and dust samples of ZSA averaged at −0.37 ± 0.37‰ (−0.87‰–0.19‰, n = 5), −0.98 ± 0.12‰ (−1.09‰–0.82‰), −0.90 ± 0.57‰ (−1.98‰–0.08‰, n = 6), and −0.78 ± 0.15‰ (−0.93‰–0.63‰), respectively (Table A.2). No significant MIF was observed in these samples. δ^{202}Hg values in coal and soil samples of CFPPA averaged at −1.38 ± 0.42‰ (−1.89‰–0.85‰, n = 5) and −1.63 ± 0.33‰ (−2.05‰–1.08‰, n = 6), respectively. No significant MIF was found in coal samples (−0.03 ± 0.06‰, n = 5), but negative Δ^{199}Hg values were observed in soil samples (−0.31 ± 0.05‰, n = 6). Previous studies found that coal combustion products showed large variations of δ^{202}Hg (−0.99‰ to −0.47‰), but small variations of Δ^{199}Hg (near zero) (Tang et al., 2017; Sun et al., 2013; Sun, 2019). Therefore, Δ^{199}Hg values were adopted to trace the sources of soil Hg in CFPPA. δ^{202}Hg values in gold ore, soil, and dust samples of GMA averaged at 0.31 ± 0.25‰ (0.03‰–0.65‰, n = 7), −1.20 ± 0.53‰ (−2.00‰ to −0.08‰, n = 7), and −0.53 ± 0.18‰ (−0.71‰, −0.35‰), respectively. A portion of the soil samples showed variations of Δ^{199}Hg form −0.33‰ to 0.02‰, with the mean of −0.13 ± 0.11‰ (n = 7), but no significant MIF was observed in gold ore and dust samples. δ^{202}Hg values in soil samples of MMA averaged at −0.89 ± 0.25‰ (−1.30‰–0.62‰, n = 7) and δ^{202}Hg values in dust samples were −0.98‰ and 0.20‰ (n = 2), while no significant MIF was found in soil samples.

Previous studies have demonstrated that surface soil can preserve the isotopic fingerprints of Hg from emission sources (Estrade et al., 2011; Feng et al., 2013; Zhang et al., 2013). The plot of soil Δ^{199}Hg vs δ^{202}Hg in the four areas is shown in Fig. 3. The soil Hg isotopic compositions in CFPPA and MMA are relatively concentrated in the plot, which indicated the existence of a significant source impacting on soil Hg in the two areas. Negative soil Δ^{199}Hg values in CFPPA (−0.28 ± 0.18‰) were comparable with those reported for deep forest soils in China (−0.17 ± 0.14‰, Wang et al., 2019), indicating that geological background value of Δ^{199}Hg dominated those found in soil Hg in CFPPA. By contrast, a scattered pattern of soil Hg isotopic compositions in GMA and ZSA may reflect complex pollution sources and disturbances. These results illustrated that Hg isotopic compositions could be useful tools in tracing pollution sources of soil Hg in the typical Hg emission areas (Fig. 3).

3.4. Source apportionment

3.4.1. Hg isotope approach

A significant negative correlation (R^2 = 0.49, $p < 0.05$) was established between soil δ^{202}Hg and the reciprocal of soil THg

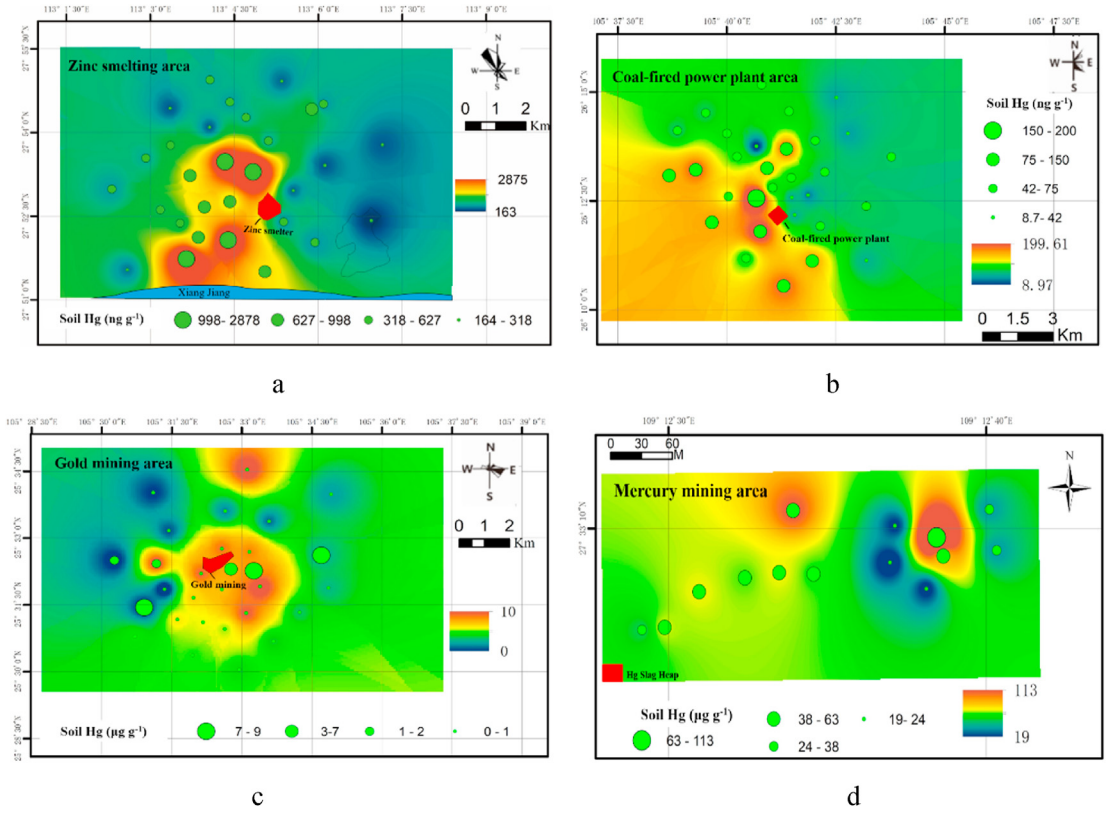

Fig. 1. Spatial distribution of soil THg in four areas. a: ZSA; b: CFPPA; c: GMA; d: MMA. The size of the dots indicates the Hg contents, and the colour of the base map indicates the spatial distribution of the Kriging interpolation by ArcGIS 10.5. . (For interpretation of the references to colour in this figure legend, the reader is referred to the Web version of this article.)

concentration in ZSA (Fig. 4a). Based on Fig. 4a, the end member values of 1/THg and Hg isotopic composition were identified for the natural background soil (1/THg$_{nat}$: 19.2, δ^{202}Hg$_{nat}$: −1.95‰) and zinc smelting facility (defined as Zn-ore) (1/THg$_{zs}$: 0.06, δ^{202}Hg$_{zs}$: 0.19‰), respectively (Table A.2). The relative contribution from zinc smelting (F$_{zs}$) to soil Hg varied from 53% at <500 m to 87% at 1.5 km and then to 36% at ~4 km away from the source (Fig. A.3a). The average contribution from zinc smelting was 64.7 ± 13.4% for whole study area, leaving 35.3 ± 13.4% from natural background.

In CFPPA, a significant negative correlation ($R^2 = 0.57$, $p < 0.05$) was found between Δ^{199}Hg and the reciprocal of THg concentration (Fig. 4b). F$_{coal}$ and F$_{nat}$ can be calculated using the end members of isotopic composition of CFPP (coal) (1/THg$_{coal}$: 3.39, $\triangle^{199}$Hg$_{coal}$: −0.03‰, n = 5) and natural background soil (1/THg$_{nat}$: 15.2, $\triangle^{199}$Hg$_{nat}$: −0.41‰). F$_{coal}$ firstly increased and then decreased with the distance away from the CFPP, with the peak value (43%) appearing at 1.5 km (Fig. 3b). The domain average contribution of CFPP to soil Hg was 26.1 ± 12.6%, while 73.9 ± 12.6% was from geogenic origin.

In GMA, a significant negative correlation ($R^2 = 0.74$, $p < 0.05$) was observed between δ^{202}Hg and the reciprocal of THg concentration, indicating mixed effects of gold mining and geogenic sources (Fig. 4c). The end members of gold mining and natural sources were assigned as the average value of gold ore samples (1/THg$_{gold}$: 0.03, δ^{202}Hg$_{gold}$: 0.31‰) and background soil (1/THg$_{nat}$: 3.73, δ^{202}Hg$_{nat}$: −2.00‰), respectively. Similar to the cases in CFPPA and ZSA, the relative contribution from the gold mining facilities to soil Hg firstly increased and then decreased with the distance to the mining site, with the peak value (84%) appeared at 1.5 km (Fig. A.3c). The domain average contribution from gold mining to soil Hg is estimated to be 40 ± 19.9%, leaving 60 ± 19.9% from natural background contributions.

In MMA, three source categories were identified, including unroasted Hg ore, Hg calcine, and the geogenic background. Negative correlations were observed between δ^{202}Hg and the reciprocal of THg concentration of calcine ($R^2 = 0.65$, $p < 0.05$) and Hg ore ($R^2 = 0.46$, $p < 0.05$) (Fig. 4d). The end member values were assigned to unroasted Hg ore (1/THg$_{ore}$: ~0, δ^{202}Hg$_{ore}$: −0.92‰), Hg calcine (1/THg$_{cal}$: 0.01, δ^{202}Hg$_{cal.}$: 0.53‰), and natural sources (1/THg$_{nat}$: 0.52, δ^{202}Hg$_{nat}$: −1.30‰). The relative contributions to soil Hg were estimated to be 77.6 ± 12.0% from the unroasted Hg ore, 14.6 ± 7.50% from the Hg calcine, and 7.80 ± 0.08% from the geogenic background on domain average. The relative contribution from the geogenic background decreased to 2% when soil THg increased to 113.3 μg g^{-1} (Fig. A.3d), indicating a proportional relationship between the contribution rate and the soil Hg concentration and severe impact by Hg mining activities on soil Hg at this site.

3.4.2. Receptor model analysis

In ZSA, PCA identified five PCs (denoted by PC1 to PC5) that contributed to soil Hg, explaining 81.9% of the total variance. PC1 mainly consisted of high component loadings on Hg, Cu, Zn, Cd, Pb, and Bi (Table A.3). Those elements are significantly elevated in sphalerites, fly ash, dust, and soil samples of this area (Table A.4), indicating the origin from smelting release and the pathway of atmosphere deposition. PC2, PC3, and PC4 were all assigned to the geogenic sources, with PC2 containing high loadings of Pr, Nd, Tb, Er, Sm, etc, PC3 containing high loadings of Mn, Co, Cs, and PC4 containing high loadings of Ca, Mg, Ti (Ostro et al., 2007; Zeng et al., 2009; Xia et al., 2010; Cheng et al., 2012). PC5 consisted of high components loadings related to traffic (V and Ni) (Johansson et al., 2009) and other metal processing components (Fe, Cr and Ni) (Chen et al., 2016), with the detailed interpretation given in SI. The total

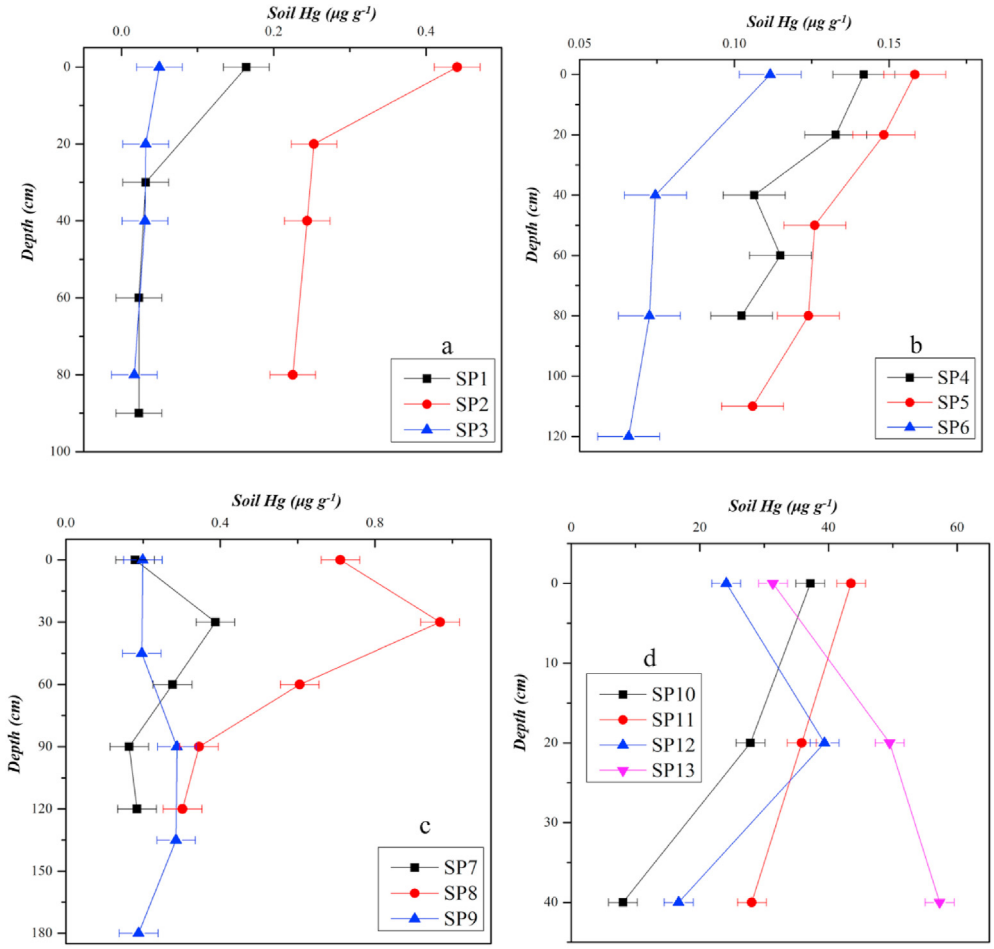

Fig. 2. Distribution patterns of THg in soil profile in four areas. a: ZSA; b: CFPPA; c: GMA; d: MMA.

APCS was 62.8% for zinc smelting source (PC1), 32.1% for geogenic source (PC2, PC3 and PC4), and 5.1% for other source (PC5).

Five source factors (denoted by F1 to F5) contributing to soil Hg were selected based on the optimal results of PMF analysis (Fig. A4a). F1 apportioned the highest contribution rate (63.1%) with the dominant components associated with zinc smelting source (e.g., Pb, Zn, Cd). F2, F3, and F4 together explained 25.1% of the total contribution. These factors were characterized by lithology components of Ca, Mg, Ti, Fe, etc, which were comparable with PCA loadings, and were thus all assigned to geogenic source. F5 was assigned to other sources, as described in SI, with a contribution of 11.8%.

In CFPPA, six PCs were identified by PCA, explaining 82.1% of the total variance. PC1 contained high loadings of Pb and low loadings of Mn, Sb, Sn (Table A.3), which could be classified as characteristic elements generated in Chinese power plants combustion processes (Fu et al., 2019), and thus PC1 might be related to the power plant emission, with the APCS of 17.8%. PC2, PC3, PC4, and PC5 contained high loadings of rare earth and lithology-related elements (e.g., Rb, Sr, La, Ca), with the APCS of 47.1% in total. PC6 consisted of high loadings of components related to other sources, which was described in SI, with the APCS of 35.1%.

Four source factors were selected in CFPPA based on PMF analysis (Fig. A.4b). F1 is dominated by Pb and Zn, which were associated with coal-fired power plant source as described above, with a contribution rate of 19.5%. F2 and F3 were characterized with comparable components of geogenic sources (e.g., Mg, Mo, La), with a contribution rate of 48.1% in total. F4 was assigned to other sources as described in SI, with a contribution rate of 32.4%.

In GMA, six PCs were obtained, explaining 86.2% of the total variance (Table A.3). In this area with Carlin-type gold deposits, characteristic heavy metals (e.g., Au, As, Sb, Hg, Tl, and S) are stored in large quantities mineralized rocks (Tan et al., 2015). Significantly elevated Hg, Sb, and Tl concentrations were detected in soil and dust samples in the present study (Table A.5). PC1 consisted of high loadings of Hg, Sb, and Tl, which was associated with the gold mining source, with the APCS of 44.3%. PC2, PC3, and PC4 all contained high loadings of geogenic elements, such as Ba, Ca, Mo, Fe, U, Cd and Pb, and concentrations of those elements in soil were comparable with local background values (Table A.5), with the total APCS of 29.5%. PC5 and PC6 were characterized by other sources, with the total APCs of 26.2%.

Four source factors were selected in GMA based on PMF analysis (Fig. A.4c). F1 is characterized by high loadings of gold mining elements, such as Hg, Sb, and Tl, with a contribution of 40.6%. F2 and F4 were characterized by geogenic components (e.g., Ca, Mo, Ti, etc) as described in PCA, with a total contribution of 52.8%. F3 was assigned to the other sources as described in SI, with a contribution rate of 6.6%.

In MMA, three PCs were identified, explaining 96.2% of the total variance (Table A.3). In this area, ore and dust samples were characterized with high contents of Cu, Zn, Cd, Pb, and Hg (Table A.6). Soil samples contained significant amounts of Cu, Cd, and Pb, which might correlate to the release from local mining. PC1 consisted of high loadings of Cu, Zn, Cd, Pb and Hg, associated with

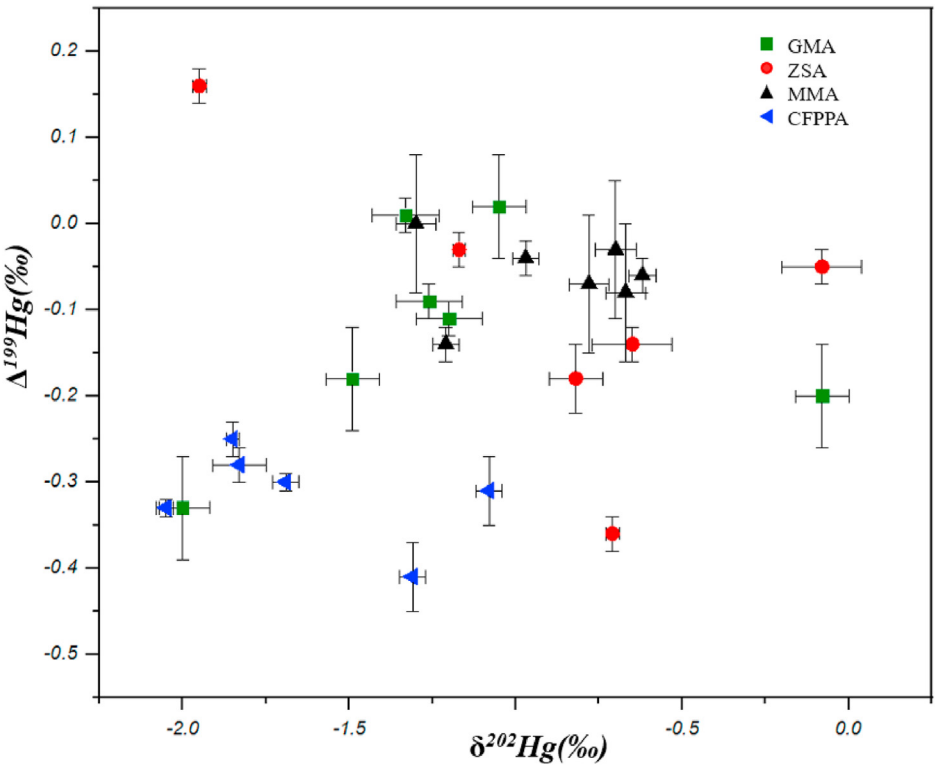

Fig. 3. Plot of Hg isotope composition of soils in four areas.

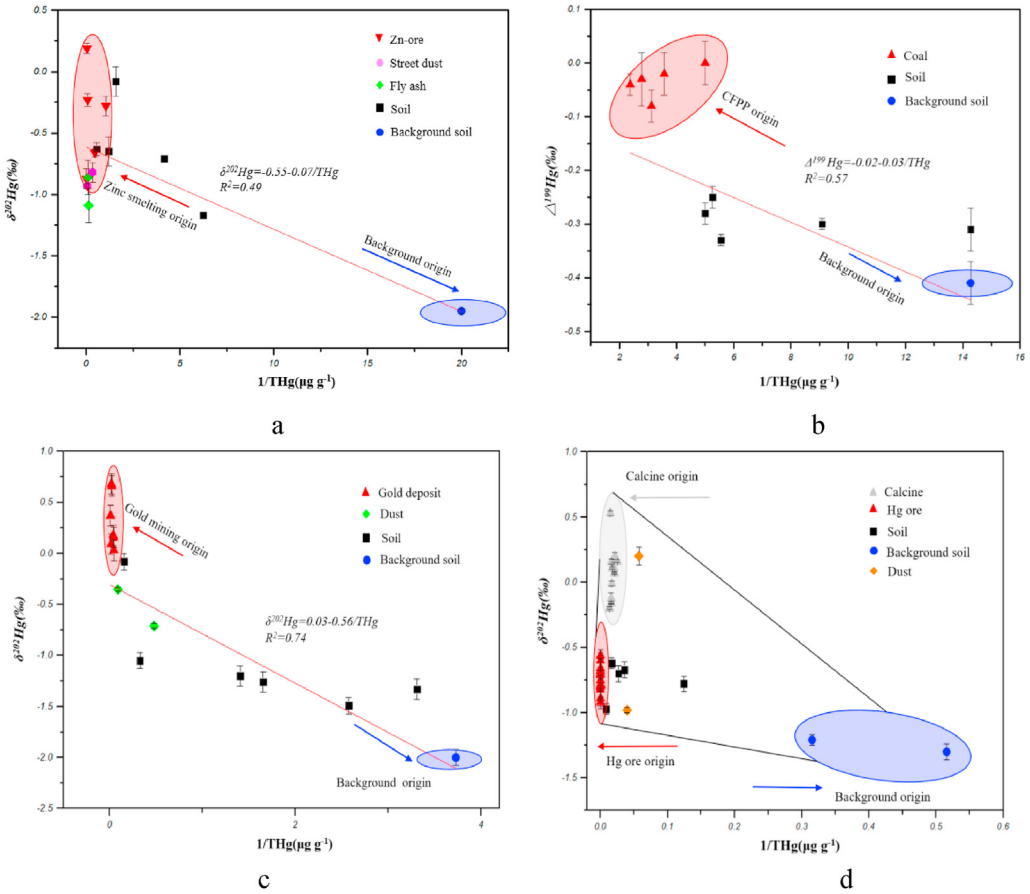

Fig. 4. Plot of Hg isotopic composition vs 1/THg in four areas. a, c, d: δ^{202}Hg vs 1/THg; b: Δ^{199}Hg vs 1/THg; a portion of Hg isotope data in Zn-ore samples were adopted from Yin et al. (2016); a portion of Hg isotope data in coal samples were adopted from Yin et al. (2014); a portion of Hg isotope data in gold deposit samples were adopted from Yin et al. (2019); all the Hg isotope data of calcine and Hg-ore samples were adopted from Yin et al. (2013).

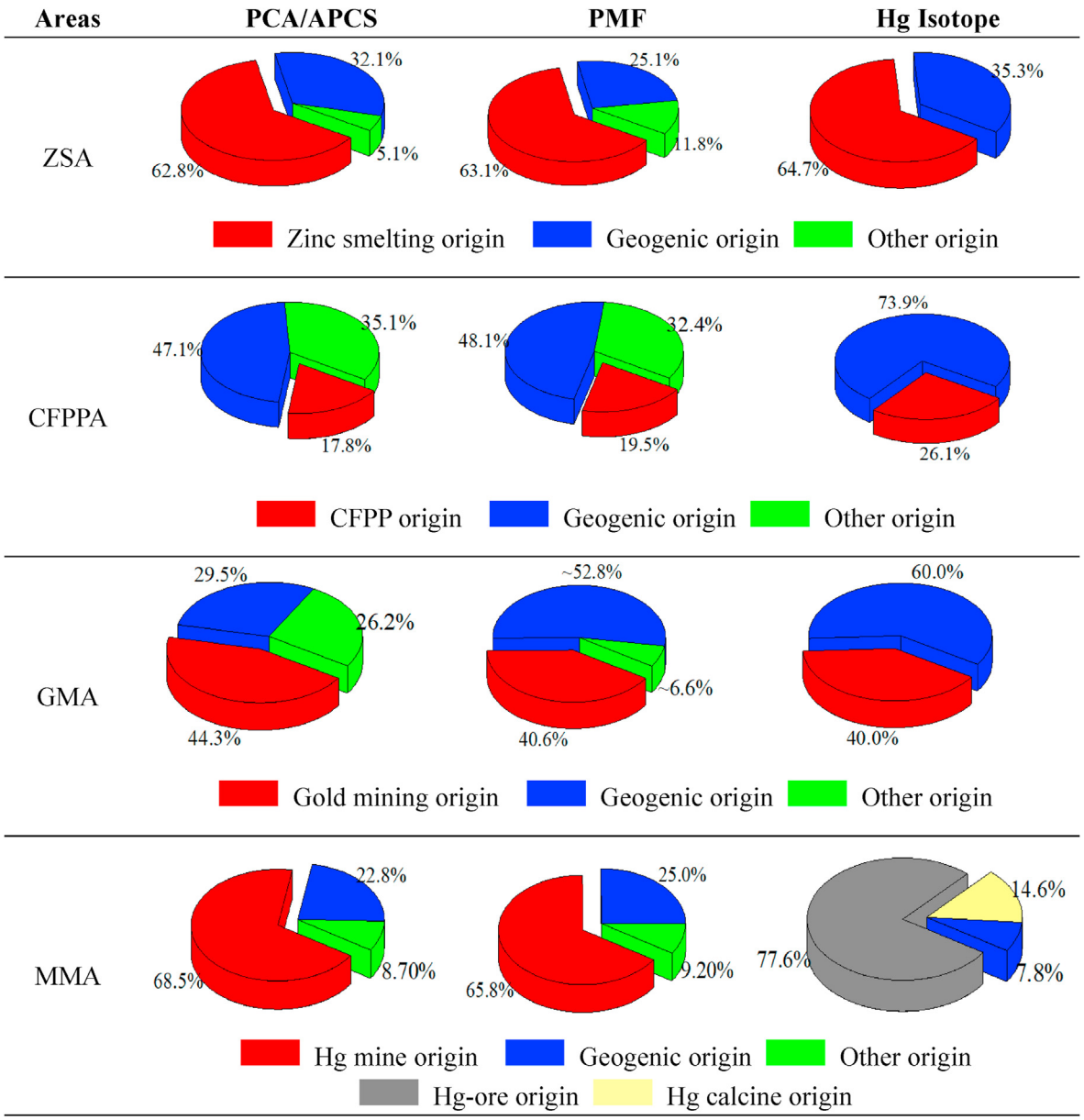

Fig. 5. Comparison of results of source apportionment by different methods.

characteristic of mining source, with a contribution of 68.5%. PC2 correlated with V, Cr, and Ba, which were comparable with background geogenic value (Table A.6), with a contribution of 22.8%. PC3 was assigned to other source, with a contribution of 8.70%.

Three source factors were selected in MMA based on PMF analysis (Fig. A.4d). F1 was characterized by mining components of Zn, Cd, Pb, and Hg, with a relative contribution of 65.8%. F2 was correlated with geogenic components of V, Mo, and Ba, with a contribution rate of 22.5%. F3 was assigned to other source, as described in SI, with a contribution rate of 9.20%.

3.4.3. Comparison between different methods

In ZSA, the zinc smelter was identified as the biggest contributor to soil Hg in the surrounding areas, and the estimated relative contributions were highly consistent between the three methods, e.g., 62.8%, 63.1%, and 64.7% by PCA/APCS, PMF, and Hg isotope approaches, respectively (Fig. 5). However, these percentage contributions were lower than previously estimated results for the same smelter (73–92%) (Wu et al., 2014), likely due to different methods used in the previous study. In GMA, the estimated relative contributions of gold mining to soil Hg were also highly consistent between the three methods, e.g., 44.3%, 40.6%, and 40.0% by PCA/APCS, PMF, and Hg isotope approaches, respectively. In CFPP, the estimated relative contributions of CFPP to soil Hg were only moderately consistent between the three models, e.g., 17.8%, 19.5%, and 26.1% by PCA, PMF, and Hg isotope approaches, respectively. In MMA, the estimated relative contributions from the Hg mining to soil Hg were much higher by Hg isotope approach (92.2%) than by PCA and PMF (68.5% and 65.8%, respectively). We speculated that such big differences may be caused by high atmospheric Hg deposition in the MMA and the fact that the receptor models (PCA and PMF) could not distinguish the rate of Hg deposition to soil based on trace elements analysis.

4. Conclusions

This study revealed soil Hg pollution caused by four different types of anthropogenic emission sources. Serious soil Hg pollution was found in Hg mining area, moderate soil Hg pollutions in gold mining and zinc smelting areas, and light soil Hg pollution in coal-fired power plant area. Soil Hg spatial distributions indicated atmospheric deposition patterns, with the peak values appearing at about 1.5–2.0 km away from emission sources in ZSA, CFPPA, and GMA. Isotopic composition approaches were illustrated to be useful tools in tracing pollution sources of soil Hg in the typical Hg emission areas. These areas can be considered as hotspots of soil Hg pollution. Anthropogenic Hg emissions should be reduced in Hg mining, zinc smelting, and gold mining industries. Soil remediation is also needed to reduce Hg bioaccumulation in agricultural crops and associated human health risks in these areas. The impacts of other anthropogenic Hg emission sectors to soil Hg pollution should also be investigated in future studies.

CRediT authorship contribution statement

Zhengcheng Song: performed experimental works, Data curation, evaluated the data, wrote the manuscript. **Chuan Wang:** performed experimental works, Data curation, evaluated the data, wrote the manuscript. **Li Ding:** performed experimental works. **Min Chen:** performed experimental works. **Yanxin Hu:** performed experimental works. **Ping Li:** conceived and designed the study, performed experimental works, Data curation, evaluated the data, wrote the manuscript. **Leiming Zhang:** wrote the manuscript, All authors read and approval to the final manuscript. **Xinbin Feng:** conceived and designed the study.

Declaration of competing interest

The authors declare that they have no known competing financial interests or personal relationships that could have appeared to influence the work reported in this paper.

Acknowledgements

This study was funded by the Strategic Priority Research Program of Chinese Academy of Sciences (XDB40020400), the National Natural Science Foundation of China (42077315, U1612442, and 41622208), the Youth Innovation Promotion Association, Chinese Academy of Sciences (2017442), “Light of West China” Program of Chinese Academy of Sciences, and the Social Development Project of Guizhou Province (2012–3044).

Appendix A. Supplementary data

Supplementary data to this article can be found online at https://doi.org/10.1016/j.jclepro.2020.125687.

References

Bergquist, B.A., Blum, J.D., 2007. Mass-dependent and mass-independent fractionation of Hg isotopes by photo-reduction in aquatic systems. Science 318, 417–420. https://doi.org/10.1126/science.1148050.

Biester, H., Müller, G., Schöler, H.F., 2002. Binding and mobility of mercury in soils contaminated by emissions from chlor-alkali plants. Sci. Total Environ. 284 (1–3), 191–203. https://doi.org/10.1016/S0048-9697(01)00885-3.

Blum, J.D., Bergquist, B.A., 2007. Reporting of variations in the natural isotopic composition of mercury. Anal. Bioanal. Chem. 388, 353–359. https://doi.org/10.1007/s00216-007-1236-9.

Brady, J.P., Ayoko, G.A., Martens, W.N., Goonetilleke, A., 2014. Temporal trends and bioavailability assessment of heavy metals in the sediments of Deception Bay, Queensland, Australia. Mar. Pollut. Bull. 89, 464–472. https://doi.org/10.1016/j.marpolbul.2014.09.030.

Chen, L., Liang, S., Liu, M., Yi, Y., Mi, Z., Zhang, Y., Li, Y., Qi, J., Meng, J., Tang, X., Zhang, H., Tong, Y., Zhang, W., Wang, X., Shu, J., Yang, Z., 2019. Trans-provincial health impacts of atmospheric mercury emissions in China. Nat. Commun. 10, 1484. https://doi.org/10.1038/s41467-019-09080-6.

Chen, T., Chang, Q.R., Liu, J., Clevers, J.G.P.W., Kooistra, L., 2016. Identification of soil heavy metal sources and improvement in spatial mapping based on soil spectral information: a case study in northwest China. Sci. Total Environ. 565, 155–164. https://doi.org/10.1016/j.scitotenv.2016.04.163.

Cheng, I., Zhang, L., Blanchard, P., Graydon, J.A., Louis, V.L.St, 2012. Source-receptor relationships for speciated atmospheric mercury at the remote Experimental Lakes Area, northwestern Ontario, Canada. Atmos. Chem. Phys. 12, 1903–1922. https://doi.org/10.5194/acp-12-1903-2012.

Cheng, I., Zhang, L., Blanchard, P., Dalziel, J., Tordon, R., Huang, J.Y., Holsen, T.M., 2013. Comparisons of mercury sources and atmospheric mercury processes between a coastal and inland site. J. Geophys. Res. Atmos. 118, 2434–2443. https://doi.org/10.1002/jgrd.50169, 2013.

Cheng, I., Xu, X., Zhang, L., 2015. Overview of receptor-based source apportionment studies for speciated atmospheric mercury. Atmos. Chem. Phys. 15, 7877–7895. https://doi.org/10.5194/acp-15-7877-2015.

CNEMC (China National Environmental Monitoring Center), 1990. The Soil Environmental Background Value in the People’s Republic of China. China Environmental Press, Beijing (in Chinese).

Driscoll, C.T., Mason, R.P., Chan, H.M., Jacob, D.J., Pirrone, N., 2013. Mercury as a global pollutant: sources, pathways, and effects. Environ. Sci. Technol. 47, 4967–4983. https://doi.org/10.1021/es305071v.

Estrade, N., Carignan, J., Donard, Olivier F.X., 2011. Tracing and quantifying anthropogenic mercury sources in soils of Northern France using isotopic signatures. Environ. Sci. Technol. 45, 1235–1242. https://doi.org/10.1021/es1026823.

Fang, F., Wang, Q., Li, J., 2001. Atmospheric particulate mercury concentration and its dry deposition flux in Changchun City, China. Sci. Total Environ. 281, 229–236. https://doi.org/10.1016/S0048-9697(01)00849-X.

Feng, X., Yin, R., Yu, B., Du, B., 2013. Mercury isotope variations in surface soils in different contaminated areas in Guizhou Province, China. Chin. Sci. Bull. 58, 249–255. https://doi.org/10.1007/s11434-012-5488-1.

Fu, B., Liu, G.J., Main, Md M., Sun, M., Wu, D., 2019. Characteristics and speciation of heavy metals in fly ash and FGD gypsum from Chinese coal-fired power plants. Fuel 251, 593–602. https://doi.org/10.1016/j.fuel.2019.04.055.

Fu, X., Marusczak, N., Wang, X., Gheusi, F., Sonke, J.E., 2016. Isotopic composition of gaseous elemental mercury in the free troposphere of the Pic du Midi Observatory, France. Environ. Sci. Technol. 50, 5641–5650. https://doi.org/10.1021/acs.est.6b00033.

Hu, X.F., Singh, K., Man, H., 2018. Mercury exposure, blood pressure, and hypertension: a systematic review and dose–response meta-analysis. Environ. Health Perspect. 126, 076002 https://doi.org/10.1289/EHP2863.

Huang, J.H., Guo, S.T., Zeng, G.M., Li, F., Gu, Y.L., Shi, Y.H., Shi, L.X., Liu, W.C., Peng, S.Y., 2018. A new exploration of health risk assessment quantification from sources of soil heavy metals under different land use. Environ. Pollut. 243, 49–58. https://doi.org/10.1016/j.envpol.2018.08.038.

Johansson, C., Norman, M., Burman, L., 2009. Road traffic emission factors for heavy metals. Atmos. Environ. 43, 4681–4688. https://doi.org/10.1016/j.atmosenv.2008.10.024.

Kwon, S.Y., Blum, J.D., Yin, R.S., Tsui, M.T.K., Yang, Y.H., Choi, J.W., 2020. Mercury stable isotopes for monitoring the effectiveness of the Minamata Convention on Mercury. Earth Sci. Rev. 203, 103111. https://doi.org/10.1016/j.earscirev.2020.103111.

Li, P., Feng, X.B., Shang, L.H., Qiu, G.L., Meng, B., Liang, P., Zhang, H., 2008. Mercury pollution from artisanal mercury mining in Tongren, Guizhou, China. Appl. Geochem. 13, 2055–2064. https://doi.org/10.1016/j.apgeochem.2008.04.020.

Li, P., Feng, X.B., Qiu, G.L., Shang, L.H., Li, Z.G., 2009. Mercury pollution in Asia: a review of the contaminated sites. J. Hazard Mater. 168, 591–601. https://doi.org/10.1016/j.jhazmat.2009.03.031.

Li, P., Feng, X.B., Chan, H.M., Zhang, X.F., Du, B.Y., 2015. Human body burden and dietary methylmercury intake: the relationship in a rice-consuming population. Environ. Sci. Technol. 49, 9682–9689. https://doi.org/10.1021/acs.est.5b00195.

Li, P., Du, B., Maurice, L., Laffont, L., Lagane, C., Point, D., Sonke, J.E., Yin, R.S., Lin, C.J., Feng, X.B., 2017a. Mercury isotope signatures of methylmercury in rice sample from the Wanshan mercury mining area, China: environmental implications. Environ. Sci. Technol. 51, 12321–12328. https://doi.org/10.1021/acs.est.7b03510.

Li, R., Wu, H., Ding, J., Fu, W.M., Gan, L.J., Li, Y., 2017b. Mercury pollution in vegetables, grains and soils from areas surrounding coal-fired power plants. Sci. Rep. 7, 46545. https://doi.org/10.1038/srep46545.

Li, Z.G., Feng, X.B., Li, G.H., Bi, X.Y., Sun, G.Y., Zhu, J.M., Qin, H.B., Wang, J.X., 2011. Mercury and other metal and metalloid soil contamination near a Pb/Zn smelter in east Hunan province, China. Appl. Geochem. 26, 160–166. https://doi.org/10.1016/j.apgeochem.2010.11.014.

Liu, M.D., Zhang, Q.R., Cheng, M.H., He, Y.P., Chen, L., Zhang, H.R., Cao, H.L., Shen, H.Z., Zhang, W., Tao, S., Wang, X.J., 2019. Rice life cycle-based global mercury biotransport and human methylmercury exposure. Nat. Commun. 10, 5164. https://doi.org/10.1038/s41467-019-13221-2.

Luo, L., Ma, Y., Zhang, S., Wei, D., Zhu, Y.G., 2009. An inventory of trace element inputs to agricultural soils in China. J. Environ. Manag. 90, 2524–2530. https://doi.org/10.1016/j.jenvman.2009.01.011.

2018 MEE PRC (Ministry of Ecology and Environment of the People's Republic of China). Soil Environmental Quality Risk Control Standard for Soil Contamination of Agricultural Land GB 15618—2018 (in Chinese)..

2012 MEP (Ministry of Environmental Protection of the People's Republic of China), Ambient Air Quality Standard. China Environment press, GB3095–2012, Beijing (in Chinese).
Norris, G.A., Duvall, R., Brown, S.G., Bai, S., 2014. EPA Positive Matrix Factorization (PMF) 5.0 Fundamentals and User Guide Prepared for the US. Environmental Protection Agency Office of Research and Development, Washington, DC. DC.EPA/600/R-14/108.
Ostro, B., Feng, W., Broadwin, R., Green, S., Lipsett, M., 2007. The effects of components of fine particulate air pollution on mortality in California: results from CALFINE. Environ. Health Perspect. 115, 13–19. https://doi.org/10.1289/ehp.9281.
Parks, J.M., Johs, A., Podar, M., Bridou, R., Hurt Jr., R.A., Smith, S.D., Tomanicek, S.J., Qian, Y., Brown, S.D., Brandt, C.C., Palumbo, A.V., Smith, J.C., Wall, J.D., Elias, D.A., Liang, L., 2013. The genetic basis for bacterial mercury methylation. Science 339, 1332–1335. https://doi.org/10.1126/science.1230667.
Pornsawai, P., Lisa, A.R., Gregory, J.C., 2013. Source apportionment of polychlorinated biphenyls in the sediments of the Delaware River. Environ. Sci. Technol. 47, 4277–4283. https://doi.org/10.1021/es400375e.
Roman, H.A., Walsh, T.L., Coull, B.A., Dewailly, É., Guallar, E., Dale, Hattis, Mariën, K., Schwartz, J., Virtanen, J.K., Rice, G., 2011. Evaluation of the cardiovascular effects of methylmercury exposures: current evidence supports development of a dose–response function for regulatory benefits analysis. Environ. Health Perspect. 119, 607–614. https://doi.org/10.1289/ehp.1003012.
Selin, N.E., 2009. Global biogeochemical cycling of mercury: a review. Annu. Rev. Environ. Resour. 34 (1), 43–63. https://doi.org/10.1146/annurev.environ.051308, 084314.
Song, Z.C., Li, P., Ding, L., Li, Z.G., Zhu, W., He, T.R., Feng, X.B., 2018. Environmental mercury pollution by an abandoned chlor-alkali plant in Southwest China. J. Geochem. Explor. 194, 81–87. https://doi.org/10.1016/j.gexplo.2018.07.017.
Sun, R.Y., 2019. Mercury stable isotope fractionation during coal combustion in coalfired boilers: reconciling atmospheric Hg isotope observations with Hg isotope fractionation theory. Bull. Environ. Contam. Toxicol. 102, 657–664. https://doi.org/10.1007/s00128-018-2531-1.
Sun, R.Y., Heimbürger, L.-E., Sonke, J.E., Liu, G.J., Amouroux, D., Berail, S., 2013. Mercury stable isotope fractionation in six utility boilers of two large coal-fired power plant. Chem. Geol. 336, 103–111. https://doi.org/10.1016/j.chemgeo.2012.10.055.
Tan, Q.P., Xia, Y., Xie, Z.J., Yan, J., 2015. Migration paths and precipitation mechanisms of ore-forming fluids at the Shuiyindong Carlin-type gold deposit, Guizhou, China. Ore Geol. Rev. 69, 140–156. https://doi.org/10.1016/j.oregeorev.2015.02.006.
Tang, S., Feng, C., Feng, X., Zhu, J., Sun, R., Fan, H., Wang, L., Li, R., Mao, T., Zhou, T., 2017. Stable isotope composition of mercury forms in flue gases from a typical coal-fired power plant, Inner Mongolia, northern China. J. Hazard Mater. 328, 90–97. https://doi.org/10.1016/j.jhazmat.2017.01.014.
Thurston, G.D., Spengler, J.D., 1985. A quantitative assessment of source contributions to inhalable particulate matter pollution in metropolitan Boston. Atmos. Environ. 19, 9–25. https://doi.org/10.1016/0004-6981(87)90290-3.
U.S. EPA, 2014. EPA Positive Matrix Factorization (PMF) 5.0 Fundamentals and User Guide. U.S. Environmental Protection Agency. EPA/600/R-14/108.
United Nations Environment Programme (UNEP), 2019. Global Mercury Assessment 2018. UN Environment Programme, Chemicals and Health Branch, Geneva, Switzerland.
Wang, S.X., Song, J.X., Li, G.H., Wu, Y., Zhang, L., Wan, Q., Streets, D.G., Chin, C.K., 2010. Estimating mercury emissions from a zinc smelter in relation to China's mercury control policies. Environ. Pollut. 158, 3347–3353. https://doi.org/10.1016/j.envpol.2010.07.032.
Wang, X., Yuan, W., Lin, C.-J., Zhang, L., Zhang, H., Feng, X., 2019. Climate and vegetation as primary drivers for global mercury storage in surface soil. Environ. Sci. Technol. 53, 10665–10675. https://doi.org/10.1021/acs.est.9b02386.
Wang, Z., Chen, Z., Duan, N., Zhang, X.S., 2007. Gaseous elemental mercury concentration in atmosphere at urban and remote sites in China. J. Environ. Sci. 19, 176–180. https://doi.org/10.1016/S1001-0742(07)60028-X.
World Health Organization (WHO), 2018. Ten chemicals of major public health concern. http://www.who.int/ipcs/assessment/public_health/chemicals_phc/en/. (Accessed 15 August 2019).
Wright, L.P., Zhang, L., Cheng, I., Aherne, J., Wentworth, G.R., 2018. Impacts and effects indicators of atmospheric deposition of major pollutants to various ecosystems – a review. Aerosol Air Qual. Res. 18, 1953–1992. https://doi.org/10.4209/aaqr.2018.03.0107.
Wu, Q.R., Wang, S.X., Wang, L., Liu, F., Lin, C.-J., Zhang, L., Wang, F.Y., 2014. Spatial distribution and accumulation of Hg in soil surrounding a Zn/Pb smelter. Sci. Total Environ. 496, 668–677. https://doi.org/10.1016/j.scitotenv.2014.02.067.
Wu, Q.R., Wang, S.X., Yang, M., Su, H.T., Li, G.L., Tang, Y., Hao, J.M., 2018. Mercury flows in large-scale gold production and implications for Hg pollution control. J. Environ. Sci. 68, 91–99. https://doi.org/10.1016/j.jes.2017.03.029.
Xia, X.H., Chen, X., Liu, R.M., Liu, H., 2010. Heavy metals in urban soils with various types of land use in Beijing, China. Environ. Pollut. 186, 2043–2050. https://doi.org/10.1016/j.jhazmat.2010.12.104.
Xia, J., Wang, J., Zhang, L., Anderson, C.W.N., Wang, X., Zhang, H., Dai, Z., Feng, X., 2020. Screening of native low mercury accumulation crops in a mercury-polluted mining region: agricultural planning to manage mercury risk in farming communities. J. Clean. Prod. 262, 121324. https://doi.org/10.1016/j.jclepro.2020.121324.
Yang, X., Wang, L., 2008. Spatial analysis and hazard assessment of mercury in soil around the coal-fired power plant: a case study from the city of Baoji, China. Environ. Geol. 53, 1381–1388. https://doi.org/10.1007/s00254-007-0747-1.
Yin, R., Deng, C., Lehmann, B., Sun, G., Lepak, R., Hurley, J., Zhao, C., Xu, G., Tan, Q., Xie, Z., Hu, R., 2019. Magmatic hydrothermal origin of mercury in Carlin-style and epithermal gold deposits in China: evidence from mercury stable isotopes. ACS Earth Space Chem. 3 (8), 1631–1639. https://doi.org/10.1021/acsearthspacechem.9b00111.
Yin, R., Feng, X., Chen, J., 2014. Mercury stable isotopic compositions in coals from major coal producing fields in China and their geochemical and environmental implications. Environ.Sci.Technlo. 48 (10), 5562–5574. https://doi.org/10.1021/es500322n.
Yin, R., Feng, X., Chen, B., Zhang, J., Wang, W., Li, X., 2015. Identifying the sources and processes of mercury in subtropical estuarine and ocean sediments using Hg isotopic composition. Environ. Sci. Technol. 49, 1347–1355. https://doi.org/10.1021/es504070y.
Yin, R., Feng, X., Wang, J., Li, P., Liu, J., Zhang, Y., Chen, J., Zheng, L., Hu, T., 2013. Mercury speciation and mercury isotope fractionation during ore roasting process and their implication to source identification of downstream sediment in the Wanshan mercury mining area, SW China. Chem. Geol. 336, 72–79. https://doi.org/10.1016/j.chemgeo.2012.04.030.
Yin, R., Krabbenhoft, D.P., Bergquist, B.A., Zheng, W., Lepak, R.F., Hurley, J.P., 2016. Effects of mercury and thallium concentrations on high precision determination of mercury isotopic composition by Neptune Plus multiple collector inductively coupled plasma mass spectrometry. J. Anal. Atomic Spectrom. 31, 2060–2068. https://doi.org/10.1039/c6ja00107f.
Zeng, G., Liang, J., Guo, S., Shi, L., Xiang, L., Li, X., Du, C., 2009. Spatial analysis of human health risk associated with ingesting manganese in Huangxing Town, Middle China. Chemosphere 77, 368–375. https://doi.org/10.1016/j.chemosphere.2009.07.020.
Zhang, H., Feng, X., Larssen, T., Qiu, G., Vogt, R.D., 2010. In inland China, rice, rather than fish, is the major pathway for methylmercury exposure. Environ. Health Perspect. 118, 1183–1188. https://doi.org/10.1289/ehp.1001915.
Zhang, H., Yin, R.S., Feng, X.B., Sommar, J., Anderson, C.W., Sapkota, A., Fu, X.W., Larssen, T., 2013. Atmospheric mercury inputs in montane soils increase with elevation: evidence from mercury isotope signatures. Sci. Rep. 3 https://doi.org/10.1038/srep03322.
Zhang, L., Wang, S.X., Wu, Q.R., Meng, Y., Yang, H., Wang, F.Y., Hao, J.M., 2012. Were mercury emission factors for Chinese non-ferrous metal smelters overestimated? Evidence from onsite measurements in six smelters. Environ. Pollut. 171, 109–117. https://doi.org/10.1016/j.envpol.2012.07.036.
Zhang, L., Wang, S., Wang, L., Wu, Y., Duan, L., Wu, Q., Wang, F., Yang, M., Yang, H., Hao, J., Liu, X., 2015. Updated emission inventories for speciated atmospheric mercury from anthropogenic sources in China. Environ. Sci. Technol. 49, 3185–3194. https://doi.org/10.1021/es504840m.
Zhao, S.L., Pudasainee, D., Duan, Y.F., Gupta, R., Liu, M., Lu, J.H., 2019. A review on mercury in coal combustion process: content and occurrence forms in coal, transformation, sampling methods, emission and control technologies. Prog. Energy Combust. Sci. 73, 26–64. https://doi.org/10.1016/j.pecs.2019.02.001.
Zheng, W., Hintelmann, H., 2010. Isotope fractionation of mercury during its photochemical reduction by low-molecular-weight organic compounds. J. Phys. Chem. A 114 (12), 4246–4253. https://doi.org/10.1021/jp9111348.
Zhou, J., Feng, X., Liu, H., Zhang, H., Fu, X., Bao, Z., Wang, X., Zhang, Y., 2013. Examination of total mercury inputs by precipitation and litterfall in a remote upland forest of Southwestern China. Atmos. Environ. 81, 364–372. https://doi.org/10.1016/j.atmosenv.2013.09.010.
Zhou, Y.T., Aamir, M., Liu, K., Yang, F.X., Liu, W.P., 2018. Status of mercury accumulation in agricultural soil across China: spatial distribution, temporal trend, influencing factor and risk assessment. Environ. Pollut. 240, 116–124. https://doi.org/10.1016/j.envpol.2018.03.086.